Chemical Engineering Journal 166 (2011) 596–606

Contents lists available at ScienceDirect

Chemical Engineering Journal

journal homepage: www.elsevier.com/locate/cej

Evaluation of systems coupling vacuum membrane distillation and solar energy for seawater desalination

Jean-Pierre Mericq[a], Stéphanie Laborie[b,*], Corinne Cabassud[c]

[a] Université de Toulouse, INSA,UPS,INP, LISBP, 135 Avenue de Rangueil, F-31077 Toulouse, France
[b] INRA, UMR792 Ingénierie des Systèmes Biologiques et des Procédés, F-31400 Toulouse, France
[c] CNRS, UMR5504, F-31400 Toulouse, France

ARTICLE INFO

Article history:
Received 26 July 2010
Received in revised form 8 November 2010
Accepted 8 November 2010

Keywords:
Seawater desalination
Vacuum membrane distillation
Solar energy
Salinity gradient solar pond
Solar collector

ABSTRACT

Vacuum membrane distillation (VMD) is a hybrid membrane-evaporative process which has been shown to be of interest for seawater desalination. The main drawback of this process is the relatively high energy requirement linked to the need to heat the feed water. A way to solve this problem could be the use of a renewable source such as solar energy to provide the heat energy required. Two solutions of solar energy use are investigated in this paper: salinity gradient solar ponds (SGSP) and solar collectors (SC). For each solution, two configurations were studied. The first was based on pre-heating the feed seawater before the membrane process while the second used a membrane module directly coupled with solar energy, i.e. a membrane submerged in an SGSP or an SC integrated at the surface of the membrane module. VMD process simulations were carried out for the four different configurations with VMD modelling software previously developed and adapted to the different combinations. Simulation results showed that immersing the membrane module directly in an SGSP could induce marked concentration and temperature polarisation phenomena that reduced fluxes. Turbulence had to be created in the feed seawater to reduce polarisations and this option was difficult to combine with an SGSP. The most interesting solution seemed to be the use of SC. High fluxes of 140 L h^{-1} m^{-2} could be reached (for a vacuum pressure of 500 Pa and a membrane with a Knudsen permeability of 1.85×10^{-5} s $mol^{1/2}$ m^{-1} $kg^{-1/2}$).

1. Introduction

Over the last few years, reverse osmosis (RO) has become the leading technology for new desalination installations [1]. In 2005, the Ashkelon plant in Israel became the world's largest reverse osmosis desalination plant, with a production capacity of 330,000 m^3 d^{-1} [2], and some other large RO plants are now at the stage of projects in the world. In seawater desalination, the trend is mainly to build large centralized desalination plants, as they are more economical and suitable for areas of high population density [3]. However, numerous low-density population areas lack fresh water there is thus also a need for small-scale, stand-alone desalination units to be located in dry, rural areas. For that purpose, membrane distillation (MD) is of real interest. MD is a hybrid of thermal distillation and membrane processes [4,5]. The driving force is the water partial pressure difference between the two sides of a hydrophobic porous membrane. In MD, water is vaporised from the heated feed solution and vapour diffuses through the pores of the membrane by various mechanisms. MD systems can be classified in four different configurations: direct contact MD (DCMD), air-gap MD (AGDM), sweeping gas MD (SGMD) and vacuum MD (VMD), three of which, DCMD, AGMD and VMD, are the best suited for desalination applications. The condensing liquid is in direct contact with the membrane surface in DCMD, whereas an air gap separates the permeate from the membrane in AGMD. Finally, in VMD, low pressure is applied on the permeate side and the steam condensation takes place outside the membrane module. MD has proved to be an interesting solution for seawater desalination at bench-scale [6–8]. Recently, pilot tests on the Memstill® process over a thousand hours have shown the potential of membrane distillation for desalination, with no scaling or biofouling problems during the pilot testing periods [9].

However, one of the main drawbacks of the MD for seawater desalination is the total energy requirement. In the case of VMD for instance, energy requirements are of three types (Fig. 1):

i) the heat energy requirement i.e. the energy needed to heat the seawater on the membrane feed side;
ii) the circulation energy requirement i.e. the energy needed to circulate the seawater on the membrane feed side;
iii) the vacuum energy requirement i.e. the energy needed to apply the low pressure on the membrane permeate side.

* Corresponding author. Tel.: +33 5 61 55 92 87; fax: +33 5 61 55 97 60.
E-mail addresses: jpmericq@gmail.com (J.-P. Mericq), stephanie.laborie@insa-toulouse.fr (S. Laborie), cabassud@insa-toulouse.fr (C. Cabassud).

1385-8947/$ – see front matter © 2010 Elsevier B.V. All rights reserved.
doi:10.1016/j.cej.2010.11.030

Nomenclature

C_f	feed mean concentration (mol L^{-1})
C_{fi}	feed inlet concentration (mol L^{-1})
C_{fo}	feed outlet concentration (mol L^{-1})
C_m	concentration at the membrane (mol L^{-1})
CPC	concentration polarisation coefficient
h_f	heat transfer coefficient in feed water (W m^{-2} K^{-1})
J_{water}	permeate flux (L h^{-1} m^{-2})
K_l	mass transfer coefficient in feed water (m s^{-1})
K_M	Knudsen permeability coefficient (s $mol^{1/2}$ m^{-1} $kg^{-1/2}$)
M_{water}	water molar mass (kg mol^{-1})
p^*_m (T_m)	pure water partial pressure at T_m (Pa)
P_p	permeate pressure (Pa)
T_f	feed mean temperature (in the bulk) (°C)
T_{fi}	feed inlet temperature (in the bulk) (°C)
T_{fo}	feed outlet temperature (in the bulk) (°C)
T_m	feed temperature (at the membrane) (°C)
TPC	temperature polarisation coefficient
v	feed inlet velocity (m s^{-1})
α_{water}	water activity coefficient
ρ_l	feed density (kg m^{-3})
ΔH_v	molar vaporization latent heat (J mol^{-1})
Re	feed Reynolds number
AGMD	air gap membrane distillation
DCMD	direct contact membrane distillation
MD	membrane distillation
SC	solar collectors
SGSP	salinity gradient solar pond
VMD	vacuum membrane distillation

The energy recovery was not taken into consideration in the present work but must obviously be considered in VMD (cooling and condensation of the vapour permeate for instance).

Fig. 1 gives an example of these energy requirements for seawater desalination for two temperatures: 30 and 70 °C, in given operating conditions. The heat energy requirement makes up more than 98% of the total energy requirements and increases drastically with temperature. This statement is also true for the other MD configurations (DCMD, AGMD). Thus membrane distillation (MD) could be economically competitive in situations where renewable energy resources, such as solar energy, are available.

Hogan et al. [10], among the first to couple MD with solar energy, demonstrated the feasibility of the process in the case of DCMD. The MD process appeared to be compatible with the transient nature of the energy source. Banat et al. [11] integrated a DCMD module into a solar still to produce potable water from simulated seawater. The solar still was used for preheating the feed of the membrane module and also for direct potable water production. They investigated the sensitivity of the permeate flux to the brine temperature, flow rate, salt concentration and solar radiation. The contribution of the MD to the total flux of produced water was more than 80%. AGMD has also been studied [12–16]. Koschikowski et al. [13] discussed the design and development of a stand-alone MD system powered by solar thermal collectors specially designed for solar desalination. Simulation calculations for spiral-wound membranes were carried out and results showed that a very simple, compact system with a collector area of less than 6 m^2 could distil 120–160 L of water during a day in the summer in a southern country.

In the framework of the European project SMADES, several systems have been developed and installed. Six compact systems, coupling 7 m^2 of solar collectors and MD, with daily capacities between 60 and 150 L have been installed and operated in different countries [14]. Long-term performance tests demonstrated a durable operation even with very low maintenance. An autonomous, solar-driven, MD pilot unit was operated in the south of Jordan with real seawater [15]. The solar collectors, with an area of 72 m^2, heated the feed of DCMD modules. The flux obtained varied between 2 and 11 L d^{-1} m^{-2} of collector area. Recently, the MEDESOL project was initiated to develop a solar multi-stage AGMD concept for seawater desalination [16]. The heat source will be a parabolic solar concentrator intended to provide a capacity

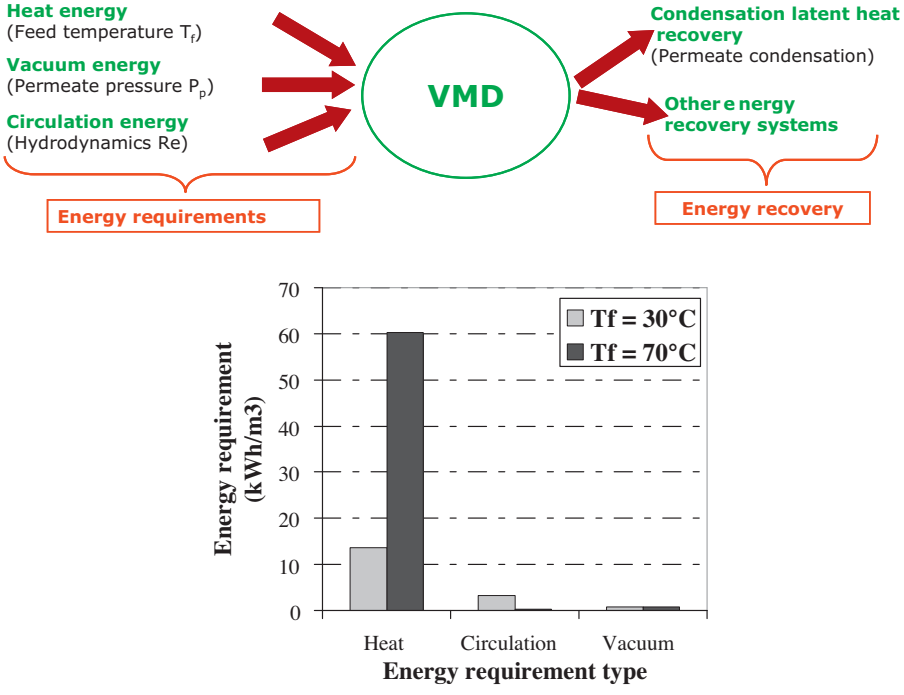

Fig. 1. Energy requirements in VMD seawater desalination: types and values (kWh m^{-3}) for $Pp = 500$ Pa and $v = 1.2$ m s^{-1}.

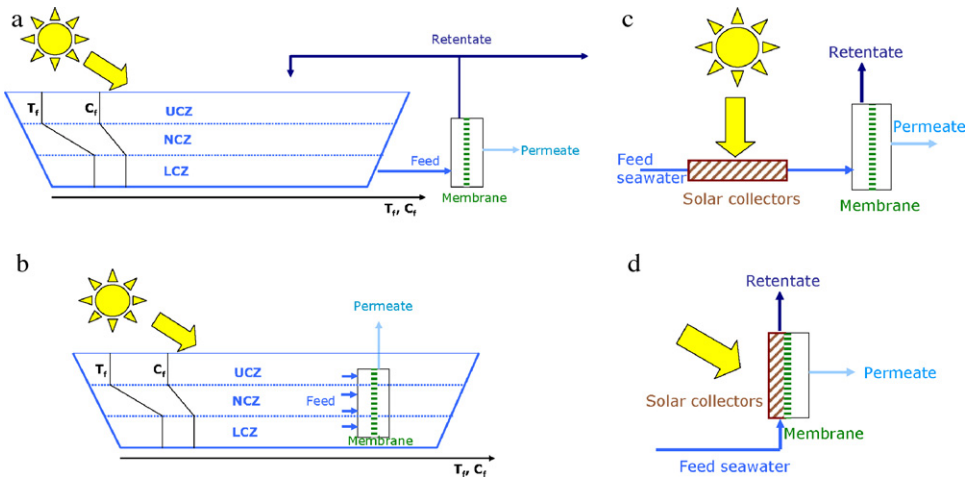

Fig. 2. Configurations of coupling VMD and solar energy: (a) membrane module fed by water taken from the SGSP (Configuration A); (b) membrane module submerged in the SGSP (Configuration B); (c) membrane module fed by water heated by SC (Configuration C); and (d) SC heating seawater directly on membrane module (Configuration D).

in the range of 0.5–50 $m^3\,d^{-1}$. Tests under real conditions will be performed in Spain and Mexico.

Concerning VMD, a recent study has focused on a solar-heated hollow-fibre-based VMD system, designed and tested by Wang et al. [17]. The largest permeate flux obtained was 32.19 $kg\,h^{-1}\,m^{-2}$ of membrane area (with an 8 m^2 solar energy collector). This study proved the feasibility of producing potable water by means of a hollow-fibre VMD module coupled with a solar energy collector.

Although the majority of studies concern the use of solar collectors to provide energy, another way to couple MD with solar energy could be to use a salinity-gradient solar pond (SGSP). SGSP allow solar energy collection combined with economical, long-term heat storage. Practical solar pond technology was first developed in the late 1950s. A considerable number of theoretical and experimental studies have been done to analyse the behaviour and predict the performance of SGSP [18–22]. An SGSP consists of three main layers: the top layer (upper convective zone, UCZ), which is close to atmospheric temperature and has a low salt concentration; the intermediate layer (non convective zone, NCZ), where there is a salinity gradient which induces a temperature gradient. Convection is suppressed in this zone. This layer provides isolation for the heat storage in the layer below: the deeper layer (lower convective zone, LCZ). This zone can provide thermal energy at temperatures ranging between 50 and 90 °C.

SGSP powered desalination has been studied at the University of Texas at El Paso since 1987. Walton et al. [23] studied the desalination performance of an AGMD system using low-grade thermal energy supplied by a salt-gradient solar pond. Experiments were performed with NaCl solutions at concentrations between 35 $g\,L^{-1}$ ("seawater") and 269.6 $g\,L^{-1}$. Hot brine was pumped from the bottom of the solar pond and passed through a heat exchanger to preheat the NaCl solutions feeding the MD module. Flux per unit area of membrane ranged from 0 to 6 $L\,h^{-1}\,m^{-2}$. A recent theoretical study [24] on a DCMD/SGSP system showed the feasibility of providing fresh water for terminal lake reclamation. The coupled system produces water flows of 1.6 $L\,d^{-1}\,m^{-2}$ of SGSP with membrane areas ranging from 1 to 1.3 $m^2\,m^{-2}$ of SGSP.

Most of the previous studies used the solar energy to preheat the seawater feeding the MD module. New configurations can be investigated by directly coupling the heating process (by solar energy) and the desalination process (by VMD). The objective of this paper is to study and compare these different classical and new configurations for coupling solar energy/VMD to produce drinking water from seawater. The approach will be based on simulations with a VMD model previously developed and validated with experimental data [6,25].

Two solar systems will be considered and evaluated: a system in which solar energy is stored in an SGSP or a system in which the membrane module is combined with solar collectors (SC). This results in four configurations for coupling VMD and solar technologies (Fig. 2):

i) Configuration A: a membrane module fed by water taken from an SGSP (Fig. 2a)
ii) Configuration B: a membrane module submerged in the SGSP (Fig. 2b)
iii) Configuration C: a membrane module fed by seawater preheated by SC (Fig. 2c)
iv) Configuration D: a membrane module fed by seawater directly heated by SC on the membrane module (Fig. 2d)

This paper focuses mainly on the membrane distillation aspect and particularly on the influence of the configuration on VMD performance.

2. Model development

2.1. VMD modelling

The four configurations described above were simulated using a VMD model previously developed and validated with experimental data for flat sheet membranes and salty solutions in a wide range of operating conditions [6,25]. These ranges were:

- concentration (0–300 $g\,L^{-1}$)
- permeate pressure (100–10,000 Pa)
- feed temperature (20–70 °C)
- Reynolds number (0–7000)

The main hypotheses of this modelling are listed below:

- mass transfer inside the membrane pores is due only to Knudsen diffusion
- heat transfer through the membrane is due only to water vaporisation
- water vaporisation occurs at the pore inlet
- only pure water goes through membrane pores

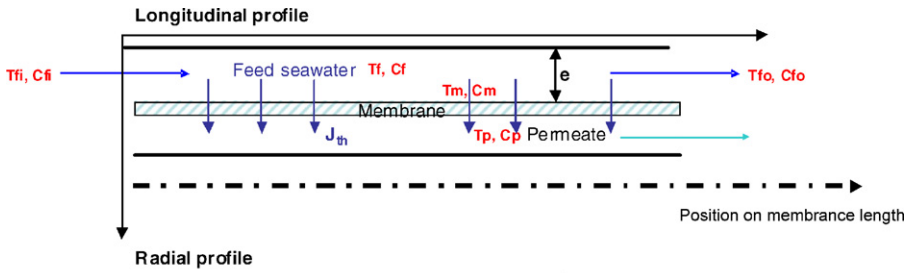

T_{fi}	Feed temperature (Inlet)
C_{fi}	Feed concentration (Inlet)
T_m	Feed temperature (Membrane)
C_m	Feed concentration (Membrane)
T_p	Permeate temperature
C_p	Permeate concentration
T_{fo}	Feed temperature (Outlet)
C_{fo}	Feed concentration (Outlet)
e	Liquid channel width

Fig. 3. Membrane module system.

- feed seawater is modelled considering only its mineral fraction, and its activity coefficient is calculated using the PHREEQC software (version 2.13.1, US Geological Survey). This modelling does not take into consideration the presence of organic matter in seawater or the possibility of salt crystallisation.

The modelling consists of the local resolution of a system of three non-linear equations: Knudsen diffusion through the membrane (Eq. (1)), mass balance on the feed side of the membrane (Eq. (2)) and thermal balance on the feed side of the membrane (Eq. (3)).

$$J_{water} = \left(\frac{K_M}{\sqrt{M_{water}}} (\alpha_{water} X_{water} p^*_m(T_m) - P_p) \right) \quad (1)$$

$$J_{water}.M_{water} - \rho_l K_l \ln\left(\frac{X_{salt,m}}{X_{salt,f}}\right) = 0 \quad (2)$$

$$J_{water}.\Delta H_v - h_f(T_f - T_m) = 0 \quad (3)$$

The configuration of the membrane module is reported in Fig. 3.

Modelling calculates the permeate vapour flow through the membrane and also determines the concentration and temperature polarisations alongside the membrane (temperature and concentration profiles in the feed bulk and near the membrane).

For all the simulations presented in this paper, a single flat-sheet membrane (1 m × 0.354 m) was considered, with a liquid channel width, e, of 1 mm. The Knudsen permeability of commercially available membranes can vary from about 2×10^{-7}–2×10^{-5} s mol$^{1/2}$ m^{-1} kg$^{-1/2}$. For the present study, the membrane had a Knudsen permeability of 1.85×10^{-5} s mol$^{1/2}$ m^{-1} kg$^{-1/2}$ (high-permeability membrane). In some cases, comparison were made with a medium-permeability membrane (with a Knudsen permeability of 3.26×10^{-6} s mol$^{1/2}$ m^{-1} kg$^{-1/2}$). Permeate pressure was fixed at 500 Pa and feed velocity at 1.2 m s^{-1}.

This VMD modelling was adapted and used in the present work to describe the four configurations and allow them to be compared.

Table 1
Solar data from Gabès in Tunisia (33°53′N; 10°06′E).

Date	December 21st	June 21st
Time of sunrise $t_{sunrise}$	7 h 21 min	5 h 09 min
Time of sunset t_{sunset}	17 h 15 min	19 h 34 min
Maximum solar irradiance E_{max} (W m^{-2})	588.24	1085.35
Water temperature T_{ci} (°C)	10.7–16.7	21.1–30.9

The solar technologies were not studied in detail. According to the configuration and solar irradiance, feed concentration and temperature were calculated from literature data, and integrated in the VMD modelling as inlet parameters. Solar data (time of sunrise, time of sunset and maximum solar irradiance E_{max}) were taken for Gabès in Tunisia (33°53′N; 10°06′E) for two dates (June 21st and December 21st), the longest and shortest days of the year (Table 1).

2.2. Coupling of SGSP/VMD modelling

2.2.1. Profiles of temperature and concentration in the SGSP

The SGSP used for the simulation was based both on a modelled SGSP [24] and an experimental SGSP designed by Fernando de la Roca Mendoza [26]. It was only calculated for December 21st. Its characteristics are given in Table 2. The depth was fixed at 1 m and the radius was 5.4 m for an area of 90 m^2.

The assumptions made for building this SGSP are listed below:

(1) SGSP is composed of seawater at different concentrations.
(2) Interfaces between UCZ and NCZ, NCZ and LCZ are stationary (salt diffusion is negligible or controlled) and the SGSP is in its steady-state.
(3) UCZ and LCZ are completely mixed (temperature and concentration are uniform and constant). Temperatures are fixed in the UCZ and LCZ at T_{UCZ} = 28 °C and T_{LCZ} = 51 °C respectively. [24]
(4) The thermal conductivity in the SGSP is constant and equal to the conductivity of water (k = 0.5 W m^{-1} °C^{-1}).

Table 2
Characteristics of the SGSP.

Zone	UCZ	NCZ	LCZ
Depth (m)	$0 < z < 0.15$	$0.15 < z < 0.45$	$0.45 < z < 1$
Seawater salt concentration (g L^{-1})	C_{UCZ} = 3 g L^{-1}	$C(z) = 300.71z - 50.122$	C_{LCZ} = 87.9 g L^{-1}
Temperature (°C)	T_{UCZ} = 28	$T(z) = 76.66z + 16.751$	T_{LCZ} = 51

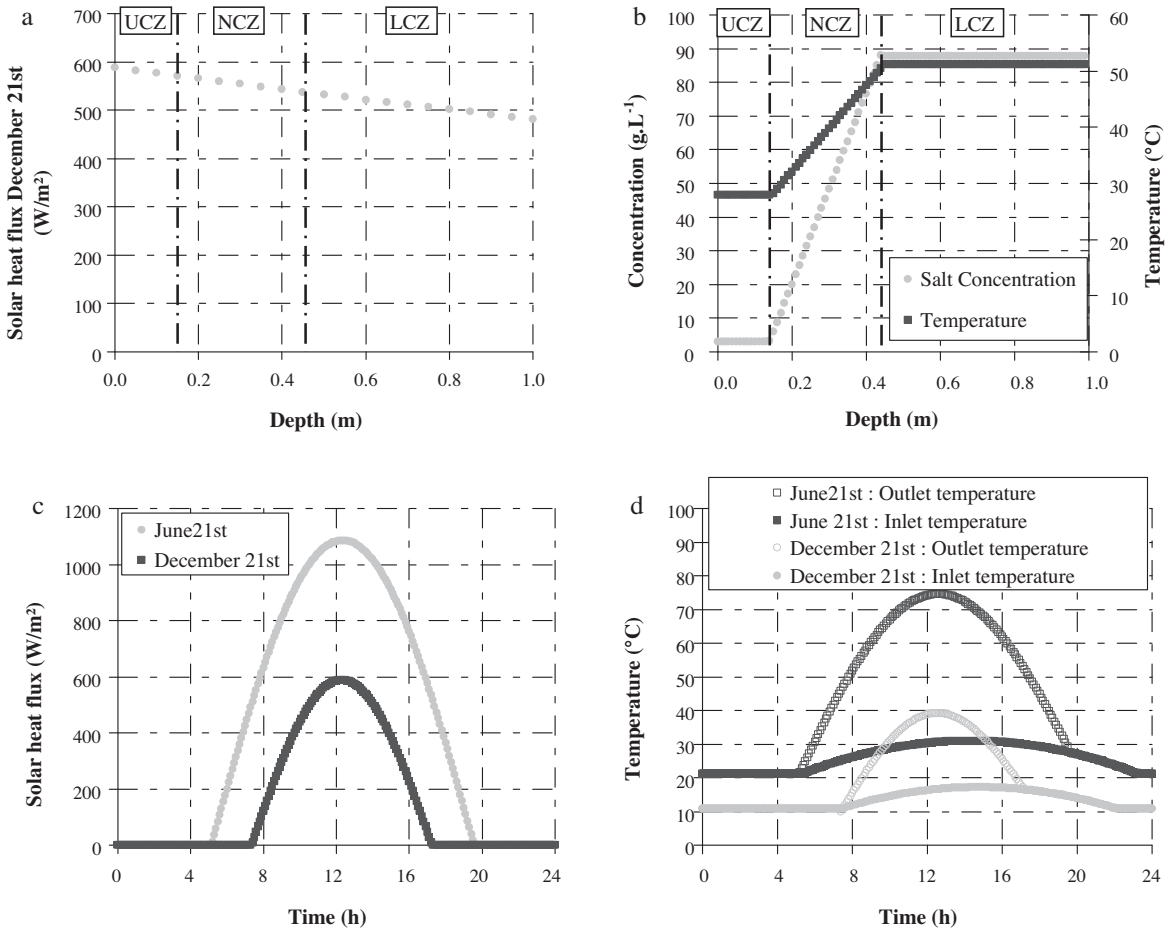

Fig. 4. Solar system characteristics: (a) solar heat flux in the SGSP; (b) temperature and concentration profiles in the SGSP; (c) solar heat flux for the SC; (d) temperatures obtained with SC during the December 21st and June 21st.

(5) The LCZ bottom and sides are thermally insulated: all the solar energy that reaches the LCZ is absorbed in this zone.
(6) No evaporation occurs in the UCZ.
(7) A global solar wave is considered with the maximum solar irradiance on December 21st and the SGSP attenuation coefficient is the water attenuation coefficient ($\lambda = 0.2\ m^{-1}$).
(8) Density gradient between UCZ and LCZ is the same as the density gradient in the SGSP of Fernando de la Roca Mendoza [26]:

$$\rho = 200z + 958.69 \tag{4}$$

Using these hypotheses, the solar radiation heat flux q was calculated at each depth z in the SGSP using Eq. (5) (Fig. 4a) [24]:

$$q(z) = E_{max}\exp(-\lambda z) \tag{5}$$

The temperature distribution in the NCZ could thus be calculated using Eq. (6) [24]:

$$T(z) = T_{LCZ} + \left(\frac{z_L - z}{z_L - z_U}\right)\left[\frac{q(z_U)}{k} - (T_{LCZ} - T_{UCZ})\right] + \left(\frac{z - z_U}{z_L - z_U}\right)\frac{q(z_L)}{k} - \frac{q(z)}{k} \tag{6}$$

The concentration distribution in the NCZ was deduced from the temperature and density distributions.

Fig. 4b shows concentration and temperature profiles obtained in the depth of the SGSP for the three different zones (UCZ, NCZ and LCZ) and for December 21st.

2.2.2. Modification of VMD modelling

In Configuration A, the membrane module is fed by water taken from the SGSP (Fig. 2a). The feed seawater temperature and concentration are constant at the membrane inlet and fixed according to the sample position in the SGSP. Along the membrane, there are temperature and concentration radial (polarisation phenomena) and longitudinal profiles (heat loss and concentration factor). This configuration induces no change in the modelling of the VMD.

In Configuration B, the membrane module is submerged in the SGSP (Fig. 2b). In this configuration, the feed seawater temperature and concentration are different according to the depth of the module in the SGSP. The feed side temperature and concentration are the seawater temperature and concentration in the SGSP. They are thus different along the membrane: temperature and concentration longitudinal profiles are determined only by SGSP profiles. As previously, there are also radial profiles (polarisation phenomena). A few changes are thus needed in the VMD modelling. First, the feed seawater is nearly static and the seawater velocity on the membrane feed side is low and negligible (value tends less than $1.5 \times 10^{-3}\ m\,s^{-1}$ and Reynolds Number inferior to 1). There is no convection effect linked to the hydrodynamics and thus mass and heat transfers on the feed side are only due to mass diffusion and heat conduction. These phenomena occur at a particular distance from the membrane to the bulk (the boundary layer or the diffusion and conduction length). This length e is the distance from the membrane to the point where the temperature and concentration reach the bulk temperature and concentration (T_f and C_f from the SGSP). It was taken to be 1 mm, the same value as the liquid channel width for the other configurations.

2.3. Coupling SC/VMD modelling

The solar irradiance $P(t)$ received by the SC was assumed to follow a sinusoidal law (Eq. (7)). E_{max} is the maximum solar irradiance received during the day, $t_{sunrise}$ and t_{sunset} are the time of sunrise and sunset respectively.

$$P(t) = E_{max} \sin\left(\pi \frac{t - t_{sunrise}}{t_{sunset} - t_{sunrise}}\right) \quad (7)$$

In Configuration C (Fig. 2c), the membrane module is fed by seawater heated by SC. In this configuration, the feed seawater temperature and concentration are constant at the membrane inlet. As for configuration A, temperature and concentration radial and longitudinal profiles exist. This configuration induces no change in the modelling of the VMD. The membrane inlet temperature (or outlet SC temperature T_{co}) can be calculated using Eq. (8) for plane SC:

$$T_{co} = \frac{\eta P(t) A_c}{m_{water} Cp_{water}} + T_{ci} \quad (8)$$

with T_{ci} the inlet feed temperature (considered to be the ambient temperature see Table 1),η the SC efficiency, $P(t)$ the solar irradiance, A_c the surface area of the collectors, m_{water} the feed mass flow, and Cp_{water} the heat capacity.

The velocity was 1.2 m s^{-1} in the membrane module defined previously, i.e. a mass flow of 0.40 kg s^{-1}. Two hypotheses were used: the SC area A_c was 90 m^2 (same area as the SGSP surface) and the efficiency η was 0.76 for plane thermal SC. Fig. 4d presents the temperature obtained at the inlet (T_{ci}) and outlet (T_{co}) of the SC. The outlet temperatures were then used in the VMD modelling.

In Configuration D, the membrane module is fed by seawater directly heated by SC on the membrane module (Fig. 2d). This configuration considers the membrane as an SC itself. There is thus no feed seawater temperature longitudinal profile since the feed seawater is considered to be homogeneously heated along the membrane and heat losses are compensated by the solar radiation heat flux. Because of heat conduction in the feed water, there is a temperature radial profile added to the radial profile of temperature due to polarisation. The water is only heated on the surface. Because of the small liquid channel width above the membrane, the hydrodynamic mixing, and the low temperature polarisation observed in VMD [27], the temperature is considered to be constant on the membrane feed side. There is so no temperature radial profile linked to the heating of the water by the surface SC.

Of course, there is also a concentration radial profile due to polarisation and a concentration longitudinal profile.

The presentation of the results is divided into three parts. The first part concerns a membrane module fed by water from an SGSP (Configuration A). The second part studies a membrane submerged in the SGSP (Configuration B). The last part focuses on coupling membrane distillation and solar thermal collectors (Configurations C and D).

3. Results and discussion

3.1. Membrane module fed by water from the SGSP (Configuration A, Fig. 2a)

3.1.1. Local permeate flux

This first part concerns the study of a membrane fed by a solution coming from an SGSP (Configuration A, Fig. 2a). The first step was to calculate the local permeate flux that could be obtained for each sampling position in the SGSP according to the local temperature and salt concentration.

Fig. 5 shows the permeate flux obtained versus the sampling position in the SGSP. The permeate fluxes expressed in L h^{-1} m^{-2} are the values after condensation of the vapour permeate. A maximum permeate flux of 71 L h^{-1} m^{-2} can be obtained. This highest permeate flux is obtained with a sampling position in the LCZ (the heat storage zone of the SGSP). In this zone, the feed temperature and salt concentration are the highest. A high temperature induces a high permeate flux but a high salt concentration induces a low permeate flux. This result confirms that the temperature has a greater effect than the concentration on the permeate flux.

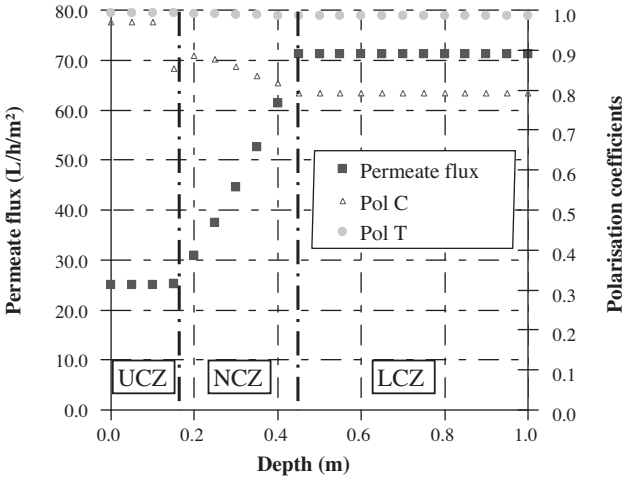

Fig. 5. Permeate flux and polarisation coefficients versus the sampled feed seawater position from the SGSP (Pp = 500 Pa, v = 1.2 m s^{-1}).

3.1.2. Concentration and temperature polarisations

Fig. 5 also presents the temperature and concentration polarisation coefficients. The temperature polarisation coefficient (TPC) is the ratio between the temperature at the membrane surface (T_m) and the feed seawater mean temperature (T_f):

$$TPC = \frac{T_m}{T_f} \qquad T_f = \frac{T_{fi} + T_{fo}}{2} \quad (9)$$

The concentration polarisation coefficient (CPC) is the ratio between the feed seawater mean concentration (C_f) and the concentration at the membrane (C_m):

$$CPC = \frac{C_f}{C_m} \qquad C_f = \frac{C_{fi} + C_{fo}}{2} \quad (10)$$

A decrease in the polarisation coefficient value indicates that the polarisation is increasing whereas polarisation coefficients close to 1 mean that there is no polarisation. It should also be noted that polarisations may exist and have only a limited effect on the permeate flux [27]. For all the sampling positions, temperature polarisation is constant and nearly insignificant but the concentration polarisation is more pronounced, especially for a sampling position in the LCZ.

Fig. 6a gives the inlet feed temperature (T_{fi}), the outlet feed temperature (T_{fo}) and the temperature close to the membrane surface (T_m) versus the sampling position in the SGSP.

Temperature polarisation is confirmed to be limited and only slight difference can be observed between the membrane and feed temperature when the temperature is the highest (sampling position in the LCZ). There is no difference between inlet and outlet feed temperature. The temperature profiles are influenced by the heat losses through the membrane: by conduction through the membrane and by water vaporisation. Permeate temperature is theorically the same as membrane temperature but can be lower in cases of heat losses toward environment. Nevertheless, thermal conductivity through the membrane is low (0.07–0.08 W m^{-1} K^{-1}) and heat losses by conduction can be negligible. Heat loss by water vaporisation increases naturally with the permeate flux rate. How-

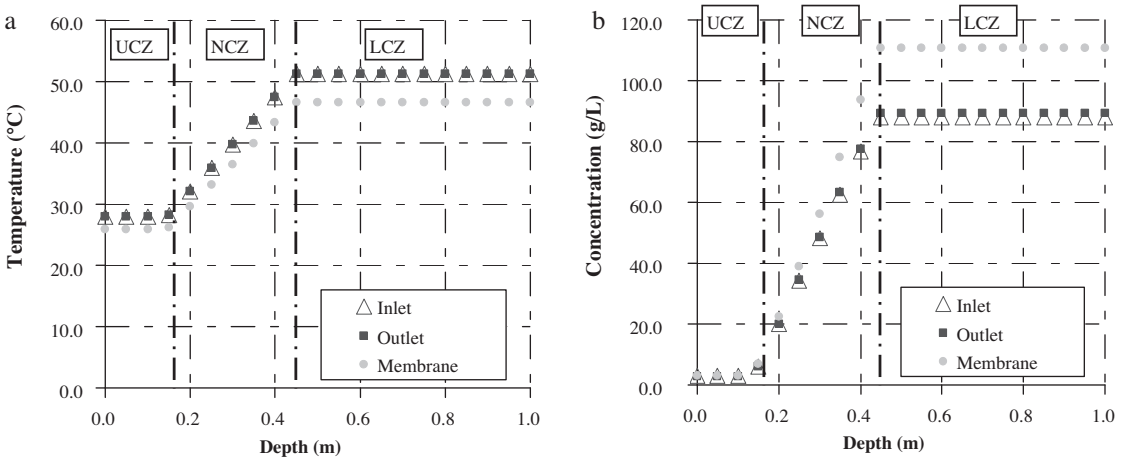

Fig. 6. (a) temperatures and (b) concentrations obtained versus the sampled feed seawater position from the SGSP (Pp = 500 Pa, v = 1.2 m s^{-1}).

ever, as the membrane length is short and its surface small, these heat losses are limited. A small polarisation temperature can exist but no temperature difference between inlet and outlet.

It must be pointed out that although temperature polarisation is lower than concentration polarisation, it has a large effect on the permeate flux rate since the permeate flux is exponentially dependent on the temperature (Antoine's Law). However, this influence stays limited.

Fig. 6b presents the inlet feed concentration (C_{fi}), the outlet feed concentration (C_{fo}) and the salt concentration close to the membrane surface (C_m) versus the sampling position in the SGSP. As for the temperature, nearly no variation between the inlet and outlet is observed for the salt concentration. This is easily explained by the water permeate flux, which is not high enough to modify the feed concentration along the membrane. However, the permeate flux is high enough to create a concentration polarisation phenomenon. A difference between the feed and membrane concentration can thus be observed, essentially for sampling positions in the LCZ.

Although polarisations are greater for the sampling position in the LCZ, higher permeate flux can be obtained. It is more interesting to use water from the LCZ to feed the membrane module. Furthermore, the stability of the SGSP will not be disturbed if feed water comes from the LCZ. The volume of the LCZ is 49.5 m^3 and the circulation flow rate is 1.52 m^3 h^{-1}. If the feed flow is not recycled toward the LCZ, LCZ volume reduction would be more than 73% per day and the LCZ would be destroyed. Since the LCZ volume is high and the increase of salt concentration in the membrane module is only 1.6%, this recycling is possible.

With a permeate flux of 71 L h^{-1} m^{-2}, the daily water production will be 603 L which represents a LCZ volume reduction of 1.2% per day. In order to prevent destabilization of this zone, maintenance must be envisaged with a supply of concentrated feed water in the LCZ.

In order to reduce polarisation effects, a high velocity can be chosen in the feed side of the membrane. For example, an increase of velocity from 1.2 to 1.9 m s^{-1} increases the permeate flux of 12% whereas circulation energy still stay low in comparison to vacuum energy (10%). Indeed, high velocities induce high turbulence and so a better stirring which reduces the concentration polarisation. The permeate flux is thus increased and the polarisation due to the high permeate flux is eliminated through greater mixing intensity..

3.2. Membrane module submerged in an SGSP (Configuration B, Fig. 2b)

3.2.1. Local profiles in the SGSP: permeate flux, temperature and concentration polarisation

Local permeate flux that could be obtained in the SGSP was calculated from temperature and concentration data versus the depth in the SGSP (Fig. 4b). It was calculated for the two different Knudsen permeabilities. Results are presented in Fig. 7.

First of all, as could be expected, a higher permeability allows higher fluxes to be reached. In the simulations,

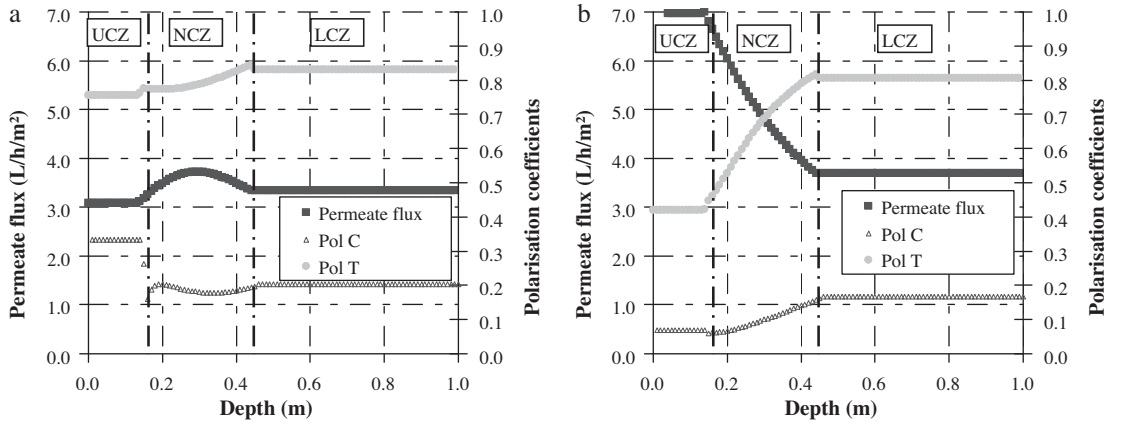

Fig. 7. Local permeate flux and polarisation coefficients in the SGSP (Pp = 500 Pa) for: (a) a 3.26×10^{-6} s mol$^{1/2}$ m^{-1} kg$^{-1/2}$ Knudsen permeability and (b) a 1.85×10^{-5} s mol$^{1/2}$ m^{-1} kg$^{-1/2}$ Knudsen permeability.

Table 3
Comparison of membrane module submerged in the LCZ with or without agitation.

Configuration	Membrane submerged in the LCZ without agitation (Configuration B)	Membrane submerged in the LCZ with agitation	Membrane fed by waters from the LCZ (Configuration A)
Permeate flux ($L\,h\,m^{-2}$)	3.7	70.6	71.2
TPC	0.81	0.99	0.99
CPC	0.17	0.79	0.79

a flux of $7.0\,L\,h^{-1}\,m^{-2}$ could be obtained locally for a $K_M = 1.85 \times 10^{-5}\,s\,mol^{1/2}\,m^{-1}\,kg^{-1/2}$ whereas, for a permeability $K_M = 3.26 \times 10^{-6}\,s\,mol^{1/2}\,m^{-1}\,kg^{-1/2}$ the maximum flux obtained was less than $4.0\,L\,h^{-1}\,m^{-2}$. Unlike the case of the previous configuration (Configuration A), the maximum permeate flux is not always located in the LCZ where temperature and concentration are the highest. In the operating conditions of this study, two cases can be obtained for the location of the maximum local permeate flux: it can be found in the NCZ (Fig. 7a) or in the UCZ (Fig. 7b) where temperature and concentration are the minimum. With the medium-permeability membrane (Fig. 7a), the maximum permeate flux is obtained at 0.3 m depth in the SGSP, i.e. in the middle of the NCZ, with a permeate flux of $4.0\,L\,h^{-1}\,m^{-2}$. Due to this high flux, the polarisation phenomena are maximum (mainly concentration polarisation). A similar flux of $3.3\,L\,h^{-1}\,m^{-2}$ is obtained in the LCZ where polarisations are smaller (polarisation coefficients are higher). It is interesting to note that the minimum permeate flux is found in the UCZ where temperature is lower. Since this zone is less concentrated, concentration polarisation is lower. However, temperature polarisation is higher which reduces the permeate flux.

With a high-permeability membrane (Fig. 7b), the maximum permeate flux is obtained in the UCZ where, although the temperature is also lower, the concentration is lower and induce a higher permeate flux. Because of this high flux, polarisation effects are greater but they do not induce too great a reduction in the permeate flux. In the LCZ, the permeate flux is nearly the same as for the medium-permeability membrane ($3.7\,L\,h^{-1}\,m^{-2}$). Concentration and temperature polarisation coefficients in the LCZ are the same for the two membranes and seem to be a very important limitation for the permeate flux. Even if the membrane permeability is increased, no increase is observed in the flux. Permeate flux thus seems to reach a saturation level.

In this configuration, feed seawater hardly moves (Reynolds lower than 1) and there is no radial convection phenomenon nor mixing. Only diffusion (for the concentration) and conduction (for the temperature) can limit the polarisation effects but these phenomena are very slow. This explains the low permeate flux that can be obtained in comparison with Configuration A. Concentration and temperature polarisations thus have an important effect on the position of the maximum permeate flux obtained. In the same way, the permeate flux value has a considerable effect on the polarisation coefficients: a high permeate flux induces polarisation effects and high polarisation effects induce a low permeate flux. These two parameters are strongly linked.

Table 3 presents simulated results for a membrane submerged in the LCZ without agitation, a submerged membrane with an agitated system and also recalls the results for a membrane fed by water from the SGSP (see Configuration A). Simulations with agitation were performed with mass and heat transfer coefficients equal to those present in a system including tangential circulation on the membrane surface (Configuration A).

Simulations clearly show that the temperature polarisation is small for the two cases (with or without agitation). In contrast, the concentration polarisation is much more significant in the case of a module submerged in an SGSP without agitation. As a consequence of this concentration polarisation effect, permeate flux obtained in mixing conditions is increased by a factor 20 compared to that obtained in non-agitated conditions. Values obtained with agitation are similar to values obtained in Configuration A. One solution could be to generate mixing to reduce these polarisations by creating a recirculation close to the membrane in order to induce some turbulence. Another option would be to set up bubbling in the feed water, which could also reduce fouling. However, these solutions could have a negative impact on the stability of the pond and leads to a high energy requirement.

3.2.2. Mean permeate flux and water production

The second step of the simulation was the calculation of the mean permeate flux and of its variation with membrane length. Only the more permeable membrane was considered here. There are two different ways to submerge the membrane module in the SGSP. The membrane module can be fixed at the top or the bottom of the SGSP. For each of these configurations, the impact of the membrane length on the permeate flux was studied up to a membrane length of 1 m. This length corresponds to a membrane with the same length as the total SGSP depth. Fig. 8 shows the mean permeate flux that can be obtained versus the membrane length. Fig. 8a represents the case of a membrane fixed at the top of the SGSP and also reports the position of the membrane bottom in the SGSP. As an example, if the membrane has a length of 0.2 m, the membrane bottom will be at a depth of 0.2 m in the SGSP. Fig. 8b shows the case of a membrane fixed at the bottom of the SGSP and also reports the position of the membrane top in the SGSP. For example, if the membrane has a length of 0.2 m, the membrane top will be at a depth of 0.8 m in the SGSP.

These two figures show that the highest fluxes are obviously achieved when the membrane passes through the portion of the SGSP where the local permeate flux is maximum, i.e. the UCZ in the present case. If the membrane is fixed at the top (Fig. 8a), the mean permeate flux decreases when the membrane length increases since the maximum permeate flux is obtained in the UCZ. The UCZ is a sensitive zone which protects the NCZ. Immersing the membrane in the UCZ can strongly reduce the thickness of this zone (if the permeate flux is high) and thus the UCZ can no longer protect the NCZ. This solution must therefore be eliminated.

For the membrane fixed at the bottom (Fig. 8b), the membrane must pass through all the SGSP (and so the NCZ) to reach the UCZ. However, only a slight increase is observed in the permeate flux ($3.4\,L\,h^{-1}\,m^{-2}$) in comparison with a membrane placed only in the LCZ ($3.3\,L\,h^{-1}\,m^{-2}$). When the membrane goes through all the SGSP, a possible destabilisation of the SGSP can occur if the NCZ concentration and temperature profiles are modified as the NCZ is an essential and very sensitive zone. Polarisation effects can destabilize the temperature and concentration profiles in the SGSP. The interesting solution for a membrane fixed at the bottom of the pond thus seems to be the location of the membrane only in the LCZ.

Fig. 8 also presents the cumulative permeate production, i.e. the water production per hour that can be obtained for a membrane fixed at the SGSP top or bottom and for different membrane lengths. As previously explained, it is better to have the membrane located only in the LCZ and so fixed at the bottom of the SGSP. For a membrane length of 0.55 m (with a width of 0.354 m), the permeate flow will be $0.7\,L\,h^{-1}$ i.e. a daily production of 16.8 L. It should also be noted that this water production does not depend on the permeability of the membrane since temperature and concentra-

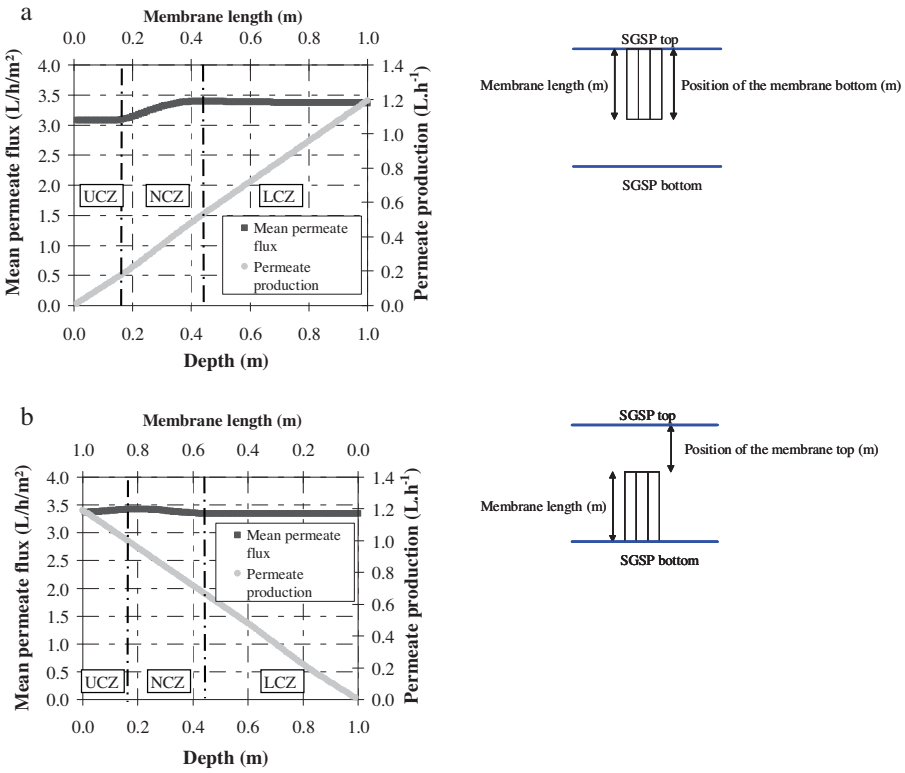

Fig. 8. Mean permeate flux and permeate production (a) for a membrane module fixed at the top of the SGSP; and (b) for a membrane module fixed at the bottom of the SGSP.

tion polarisation are the limiting factors. Membrane area must thus be maximized by increasing membrane width and using a membrane of the same length as the LCZ (0.55 m in the present case). The number of membranes can also be increased to increase the production.

Considering the water daily production, the LCZ volume reduction will be less than 0.04% by days, which prevent any destabilization of this zone. However, for long-term maintenance, a supply of concentrated feed water in the LCZ may be envisaged.

3.3. Membrane module coupled with SC (Configurations C and D, Figs. 2c and d)

This third part is dedicated to the coupling of SC and VMD. Two possibilities are available. Usually, the SC are placed upstream of the membrane module in order to heat the feed water (Configuration C, Fig. 2c). Another configuration can be envisaged, in which the feed seawater is directly heated on the membrane (Configuration D, Fig. 2d), which limits the heat loss along the membrane. This configuration considers the membrane as an SC.

3.3.1. Permeate flux and daily production

Using the temperature obtained with SC (Fig. 4d), the permeate flux was simulated for June 21st and December 21st, considering a 90 m^2 thermal SC preheating feed water (Configuration C from Fig. 2c). The results are reported in Fig. 9.

The temperature profile changes during the course of the year. The maximum daily feed water temperature is 39 °C in winter and 75 °C in summer with the same SC area. The permeate flux varies from 5.5 to 44.0 $L\,h^{-1}\,m^{-2}$ during winter and from 14.8 to 186.2 $L\,h^{-1}\,m^{-2}$ during summer. It must be noted that there is a slight permeate flux during the night since the ambient temperature is high enough to generate a transmembrane pressure difference with the vacuum pressure.

The daily water production thus ranges from 130 L (winter) to 617 L (summer). More than 64% of the water production is obtained between 10:06 and 14:30 (about 4 h 30 min of operation) for December 21st. For June 21st, 53% of the water production is obtained between 09:24 and 15:18 (about 6 h of operation) and more than 70% between 08:00 and 16:42 (about 8 h 45 min of operation). One solution to increase the winter water production despite the low temperature would be to increase the SC area in winter.

3.3.2. Effect of the feed temperature

Fig. 10a shows the permeate flux obtained with three temperatures: 30, 50 and 70 °C and for the two different configurations

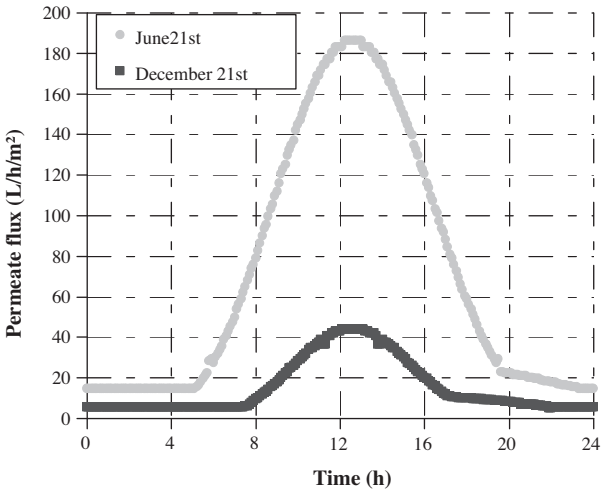

Fig. 9. Permeate flux obtained during the December 21st and the June 21st with solar collectors before the membrane module.

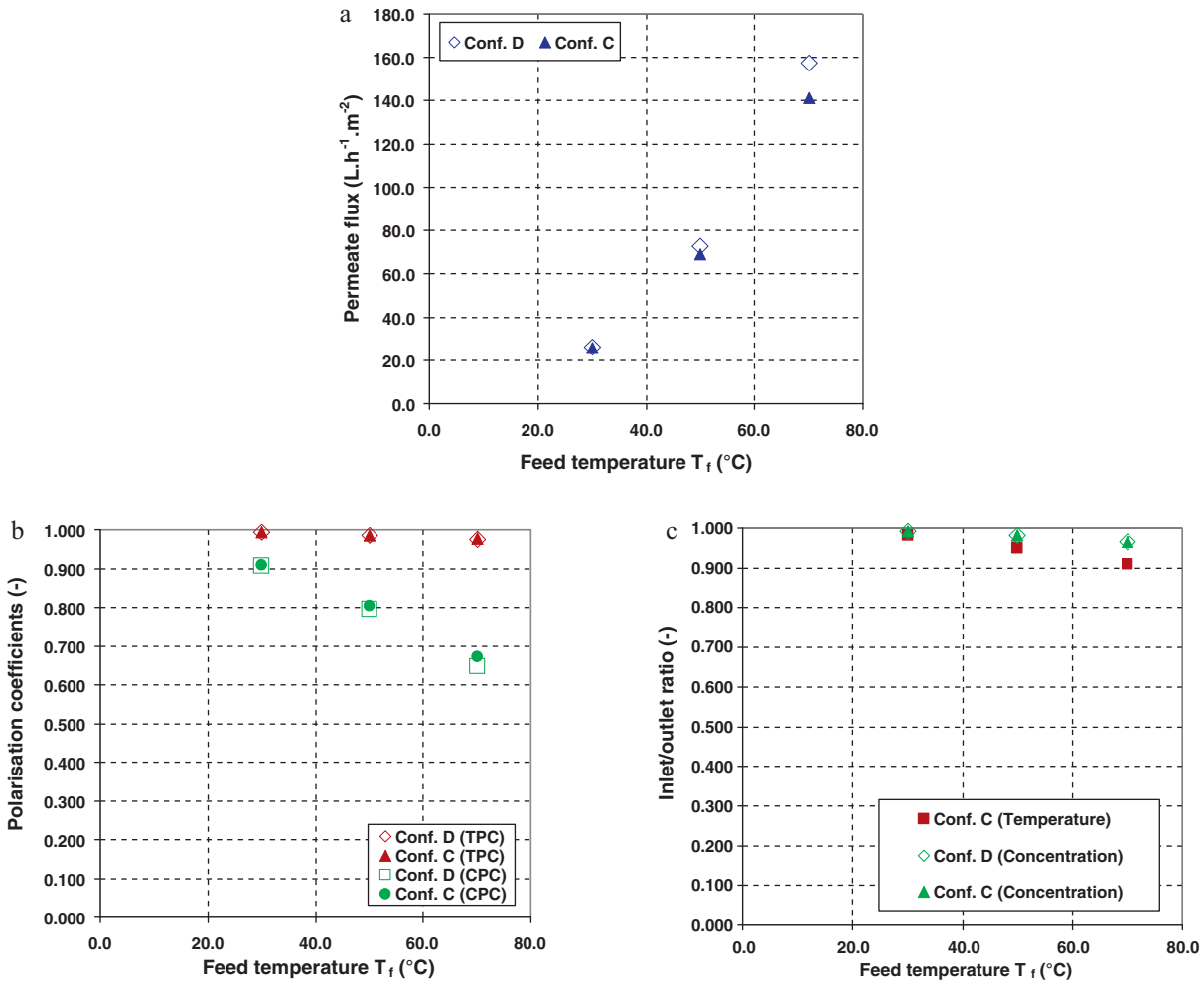

Fig. 10. (a) Permeate flux; (b) polarisation coefficients and (c) inlet/outlet ratios obtained versus the feed temperature for solar collectors before and on the membrane module (Pp = 500 Pa, v = 1.2 m s^{-1}).

using SC (Configuration C from Fig. 2c and Configuration D from Fig. 2d). These three temperatures were chosen to cover the variation of temperature that can be obtained during a day. Permeate flux varies between 30 and 150 L h^{-1} m^{-2} when temperature increases from 30 to 70 °C. No difference can be observed between the two configurations except for the highest temperature. For this value, it is shown that Configuration D yields a 14% higher permeate flux than the Configuration C. This is linked to the greater heat losses along the membrane for Configuration C (Fig. 10c). For Configuration D, the heat energy is provided throughout the length of the membrane. There is no decrease of temperature next to the membrane.

Fig. 10b shows the concentration and temperature polarisation coefficients for the two configurations. Temperature polarisation can always be neglected. Concentration polarisation is more marked when the temperature increases, in connection with the high permeate flux, but no difference can be observed between the two configurations.

Fig. 10c shows the inlet and outlet temperature and concentration ratios. For Configuration C, there is a heat loss along the membrane due to the water evaporation. It does not exist for Configuration D since the feed seawater is heated over the whole length of the membrane and compensates for the heat losses. For the two configurations, the concentration stays nearly unchanged alongside the membrane. As for Configuration A, the water permeate flux is not high enough to modify the feed concentration.

3.4. Comparison of the configurations

Table 4 compares the four configurations coupling VMD and solar energy: a membrane fed by water from the LCZ of the SGSP (Configuration A), a membrane submerged in this LCZ (Configuration B), a SC used to pre-heat the feed water (Configuration C) and a solar SC heating the feed water directly on the membrane module (Configuration D).

In Configuration B, the energy requirement is the lowest but high temperature and concentration polarisations drastically limit the permeate flux and the daily water production in comparison with the other configurations, which present nearly the same polarisation phenomena. Although Configuration A has a lower maximum feed temperature (51 °C), the daily water production is nearly the same as in Configurations C since the feed temperature in this last configuration is variable during the day and the maximum temperature (about 70 °C) is only reached for a short time. Configurations C and D require little maintenance but solar collector are more expensive than an SGSP. Conversely, Configuration A has a lower cost but needs considerable maintenance.

Configuration D gives interesting results in terms of permeate flux, concentration polarisation and energy requirement. However, as stated before, simulations of configuration D do not take the radial profile into consideration for several membrane layers and so the flux may be overestimated for this configuration. Configuration C avoids this radial profile problem since all membrane layers are

Table 4
Comparison of the four configurations.

Configuration	A (in LCZ)	B (in LCZ)	C	D
Feed temperature (°C)	51.1	51.1	70 (Variable)	70 (Variable)
Permeate pressure (Pa)	500	500	500	500
Feed velocity ($m\,s^{-1}$)	1.2	0	1.2	1.2
Permeate flux ($L\,h^{-1}\,m^2$)	71.0	3.7	141.2 (Variable)	157.7 (Variable)
TPC	0.99	0.81	0.98	0.98
CPC	0.79	0.17	0.67	0.65
Actual daily water production (L)	603	17	617	–
Energy requirement	Vacuum	Vacuum, circulation	Vacuum, circulation	Vacuum, circulation
Technical feasibility	Medium	Difficult	Easy	Difficult
Maintenance	High	High	Low	Low
Cost	Low	Low	High	High

in contact with the feed seawater at the same temperature and this seems to be the best solution.

4. Conclusion

This paper aimed to study the simulation of four configurations coupling VMD and solar energy: separating the heating and vacuum membrane distillation step or combining these two steps into one. Two configurations used an SGSP. The SGSP provided the feed water (Configuration A) or was used to submerge the membrane module (Configuration B). The two other configurations used solar thermal collectors to heat the feed seawater, either before it arrived at the membrane module (Configuration C) or directly on the membrane module (Configuration D). A VMD model previously developed was adapted to the different configurations. An estimation of the system performance – in terms of permeate flux, daily water production, temperature and concentration polarisations – was made for the four configurations to see the influence of the configuration. Energy requirements, technical feasibility, maintenance and cost were also qualitatively evaluated in order to choose one configuration. The use of SC seems to be the most interesting solution and allows a maximum permeate flux of $142\,L\,h^{-1}\,m^{-2}$ to be reached with permeable membranes. Although, the water production varies during the day and the season, a water production of $617\,L\,h^{-1}$ can be reached. A semi-industrial pilot plant is now in operation in Tunisia using VMD and plane SC in order to verify the simulation results against experiments.

Acknowledgements

This study was funded by MEDINA (http://medina.unical.it), a research project supported by the European Commission under the Sixth Framework Programme (Project number: 036997).

References

[1] L.F. Greenlee, D.F. Lawler, B.D. Freeman, B. Marrot, P. Moulin, Reverse osmosis desalination: water sources, technology and today's challenges, Water Research 42 (2009) 2317–2348.
[2] B. Sauvet-Goichon, Ashkelon desalination plant – a successful challenge, Desalination 203 (2007) 75–81.
[3] E. Mathioulakis, V. Belessiotis, E. Delyannis, Desalination by using alternative energy: review and state-of-the-art, Desalination 203 (2007) 346–365.
[4] K.W. Lawson, D.R. Lloyd, Membrane distillation review, Journal of Membrane Science 124 (1997) 1–25.
[5] M.S. El-Bourawi, Z. Ding, R. Ma, M. Khayet, A framework for better understanding membrane distillation separation process, Journal of Membranes Science 285 (2006) 4–29.
[6] D. Wirth, C. Cabassud, Water desalination using membrane distillation: comparison between inside/out and outside/in permeation, Desalination 147 (2002) 139–145.
[7] C. Cabassud, D. Wirth, Membrane distillation for water desalination: how to choose an appropriate membrane, Desalination 157 (2003) 307–314.
[8] A.M. Alklaibi, N. Lior, Membrane-distillation: status and potential, Desalination 171 (2004) 111–131.
[9] A. Jansen, J.H. Hanemaaijer, J.W. Assink, E. van Sonsbeek, Ch. Dotremont, J. van Medevoort, Pilot plants prove feasibility of a new desalination technique, Asian Water 26 (2) (2010) 22–26.
[10] P.A. Hogan, A. Sudjito, G. Fane, G.L. Morrison, Desalination by solar heated membrane distillation, Desalination 81 (1991) 81–90.
[11] F. Banat, R. Jumah, M. Garaibeh, Exploitation of solar energy collected by solar stills for desalination by membrane distillation, Renewable Energy 25 (2002) 293–305.
[12] C. Bier, U. Plantikow, Solar powered desalination by membrane distillation, IDA World Congress on Desalination and Water Science, Abu Dhabi (1995) 397–410.
[13] J. Koschikowski, M. Wieghaus, M. Rommel, Solar thermal-driven plants based on membrane distillation, Desalination 156 (2003) 295–304.
[14] J. Koschikowski, M. Wieghaus, M. Rommel, V.S. Ortin, B.P. Suarez, J.R. Rodriguez, Experimental investigations on solar driven stand-alone membrane distillation systems for remote areas, Desalination 248 (2009) 125–131.
[15] F. Banat, N. Jwaied, M. Rommel, J. Koschikowski, M. Wieghaus, Performance evaluation of the "large SMADES" autonomous desalination solar-driven membrane distillation plant in Aqaba, Jordan, Desalination 217 (2007) 17–28.
[16] J. Blanco-Galvez, L. Garcia-Rodriguez, I. Martin-Mateos, Seawater desalination by an innovative solar-powered membrane distillation system: the MEDESOL project, Desalination 246 (2009) 567–576.
[17] X. Wang, L. Zhang, H. Yang, H. Chen, Feasibility research of potable water production via solar-heated hollow fiber membrane distillation system, Desalination 247 (2009) 403–411.
[18] B. Sherman, J. Imberger, Control of a solar pond, Solar Energy 46 (2) (1991) 71–81.
[19] F. Banat, S. El Sayed, S. El-Temtamy, A transient model of a laboratory scale carnalite salt gradient solar pond, Renewable Energy 4 (8) (1994) 927–932.
[20] M. Ouni, A. Guizani, A. Belguith, Simulation of the transient behaviour of a salt gradient solar ponds in Tunisia, Renewable Energy 14 (1–4) (1998) 69–76.
[21] H. Lu, J.C. Walton, A. Swift, Desalination coupled with salinity-gradient solar ponds, Desalination 136 (2001) 13–23.
[22] M.M.O. Dah, M. Ouni, A. Guizani, A. Belghith, Study of temperature and salinity profiles development of solar pond in laboratory, Desalination 183 (2005) 179–185.
[23] J. Walton, H. Lu, C. Turner, S. Solis, H. Hein, Solar and waste heat desalination by membrane distillation, Desalination and water purification research and development program report no. 81, University of Texas at El Paso, April 2004.
[24] F. Suarez, S.W. Tyler, A.E. Childress, A theoretical study of a direct contact membrane distillation system coupled to a salt-gradient solar pond for terminal lakes reclamation, Water Research 44 (15) (2010) 4601–4615.
[25] J.P. Méricq, S. Laborie, C. Cabassud, Vacuum membrane distillation for an integrated seawater desalination process, Desalination and Water Treatment 9 (2009) 287–296.
[26] L. Fernando de la Roca Mendoza, Report on photo-thermal solar energy applied to aquaculture (Spanish), Universidad de San Carlos de Guatemala, 2003.
[27] J.P. Méricq, S. Laborie, C. Cabassud, Vacuum membrane distillation of seawater reverse osmosis brines, Water Research 44 (18) (2010) 5260–5273.